Joint Estimation of Nonlinear Dynamics and Resistance Torque for Integrated Motor-Transmission Systems via Switched $\ell \infty$ Observers With Smoothness Guarantee

Juntao Pan, Tran Anh-Tu Nguyen, Weilong Lai, Xiaoyuan Zhu, Hailong Huang

Joint Estimation of Nonlinear Dynamics and Resistance Torque for Integrated Motor–Transmission Systems via Switched L∞ Observers with Smoothness Guarantee

Article *in* IEEE Transactions on Systems Man and Cybernetics Systems · July 2023

DOI: 10.1109/TSMC.2023.3297064

CITATION
1

READS
94

5 authors, including:

Anh-Tu Nguyen
Université Polytechnique Hauts-de-France
140 PUBLICATIONS **2,084** CITATIONS
SEE PROFILE

Xiaoyuan Zhu
Southeast University (China)
46 PUBLICATIONS **804** CITATIONS
SEE PROFILE

Hailong Huang
The Hong Kong Polytechnic University
123 PUBLICATIONS **1,990** CITATIONS
SEE PROFILE

Joint Estimation of Nonlinear Dynamics and Resistance Torque for Integrated Motor-Transmission Systems via Switched ℓ_∞ Observers with Smoothness Guarantee

Juntao Pan, Anh-Tu Nguyen*, *Senior Member, IEEE*, Weilong Lai, Xiaoyuan Zhu, Hailong Huang

***Abstract*—The information of the shaft torque and the resistance torque is crucial to develop advanced control and fault diagnosis/detection schemes for electrified powertrain systems. However, reliable physical sensors for torque measurement are not affordable for commercial vehicle applications. This paper investigates the simultaneous estimation problem of the state dynamics and the resistance torque for integrated motor-transmission (IMT) systems of electric vehicles. To this end, the IMT system is first reformulated as a nonlinear switched model, where the resistance torque is considered as an unknown input (UI). This modeling reformulation allows taking into account not only the nonlinear nature of IMT dynamics but especially also the intrinsic discontinuity of the gear-shifting process. Then, we propose a nonlinear switched observer structure to simultaneously estimate the nonlinear IMT dynamics, thus the shaft torque, and the unknown resistance torque. The observer design does not require any *a priori* information on the unknown resistance torque as for the classical proportional-integral observer design, nor the well-known matching condition for UI decoupling techniques. Using Lyapunov stability theory, we derive sufficient conditions, expressed in terms of linear matrix inequality (LMI) constraints, to design a nonlinear switched observer with a guaranteed ℓ_∞ performance to mitigate the negative effect of sensor noises and disturbances. In particular, we propose to incorporate LMI-based bumps limitation conditions in the optimization-based observer design to reduce the impacts of expressive discontinuities at switching instants. Comparative studies are performed between related estimation methods to show the practical effectiveness of the proposed solution.**

***Index Terms*—Integrated motor-transmission system, torque estimation, powertrain system, switched nonlinear observer, smoothness guarantee, unknown input.**

I. Introduction

Over the last decades, electrified vehicle powertrain has been received increasing research attention to improve the performance of vehicle dynamics [1]–[5]. However, the driving range of electrified vehicles is restricted to the limited power energy provided by electrochemical batteries. Therefore, improving the efficiency of electrified powertrain systems has become a hot research topic [6]. Integrated motor-transmission (IMT) systems have been recently considered as an alternative solution for electrified powertrain to improve the power and the economy of electric vehicles [7]. With the benefit of direct-connection between multi-speed transmission and electric motor, the efficiency losses on clutches vanish, which can effectively increase the overall efficiency of electrified powertrain systems [8]. Moreover, with its gear-shift mechanism, an IMT system can constantly regulate the operating point of the motor to adapt different driving scenarios, which further increases the driveline efficiency. Hence, IMT systems have received increasing attention for electric vehicles.

The shaft torque information is crucial to develop powertrain control systems for electric vehicles [9]. For example, to improve gearshift quality, a precise information of the transmitted torque is required in [10] to develop a shift control scheme. The shaft torque information is also useful to actively cancel the driveline oscillations for driveability improvement [11]. However, physical sensors to measure the shaft torque information are too expensive for commercial applications. Hence, a great deal of research efforts have been devoted to estimate the shaft torque from the powertrain dynamics [12]–[17]. Linear observer and filtering techniques were proposed to estimate the shaft torque [18], [19], which may not provide a satisfactory estimation performance over a large operating range due to the nonlinear nature of powertrain system dynamics [13]. To deal with powertrain nonlinearities, sliding-mode shaft torque observers were proposed in [5], [20], which may require a substantial effort to mitigate the chattering impacts. A Takagi-Sugeno (TS) fuzzy unknown input observer (UIO) was proposed in [13] to estimate the transmission input and the output torque as well as the drive wheel speed of a hybrid powertrain system. Another TS fuzzy reduced-order observer was proposed in [8] to estimate the shaft IMT systems. However, the design of these TS fuzzy observers is based on the Lipschitzian property of the membership functions, which can induce a conservative estimation performance [21]. Moreover, specific matrix rank conditions must be verified for the UIO design in [13]. Note also that the time-derivative of the system output is required to construct the TS fuzzy observer in [8], which can make the estimation

J. Pan and W. Lai are with the School of Electrical and Information Engineering, North Minzu University, Yinchuan, China 750021. Email: jtpan@aliyun.com, weilonglai@aliyun.com.

A.-T. Nguyen is with the LAMIH laboratory, UMR CNRS 8201, Université Polytechnique Hauts-de-France, Valenciennes, France. A.-T. Nguyen is also with the INSA Hauts-de-France, Valenciennes, France. Email: tnguyen@uphf.fr.

X. Zhu is with the School of Mechanical Engineering, Southeast University, Nanjing 211189, China. Email: zhuxyc@gmail.com.

H. Huang is with the Department of Aeronautical and Aviation Engineering, The Hong Kong Polytechnic University, Hong Kong. Email: hailong.huang@polyu.edu.hk.

*Corresponding author: Anh-Tu Nguyen (nguyen.trananhtu@gmail.com).

performance highly sensitive to the effect of sensor noises. To overcome this drawback, the authors in [22] proposed to incorporate a recursive least square estimation algorithm in the design of a reduced-order linear observer. Despite its practical performance for transmitted driveline torque estimation in both driving and gear-shifting operations, the stability issue of the overall estimation scheme should be further investigated.

Vehicle resistance torques, *e.g.*, aerodynamic drag torque, rolling resistance torque, road gradient torque, are a major source of nonlinearities and disturbances, which bring challenges to modeling, estimation and control issues of powertrain dynamics [13], [23]. Since the measurement of resistance torques is unavailable in practice, the rolling resistance torque and the road gradient torque are generally considered as an external disturbance for shaft torque observer design [24]. Consequently, $\mathscr{H}_\infty$ filtering technique [25] has been widely adopted to mitigate the impact of these disturbances on the shaft torque estimation. However, differently from the road gradient torque and the rolling resistance torque, the aerodynamic drag torque directly depends on the wheel speed of IMT systems. Then, considering the drag torque as an external disturbance may lead to performance deterioration, especially when the impact of the wheel speed becomes dominant. To overcome this drawback, the drag torque information should be taken into account in the observer design [8]. Note also that most of estimation methods for IMT powertrain systems do not allow to recover unknown resistance torques. Moreover, the switching nature due to the gear-shifting process has not been explicitly considered in previous observer design methods.

Motivated by the above practical and theoretical issues, this paper investigates the estimation problem of IMT powertrain systems. Differently from the previous related works, the IMT system dynamics is reformulated as a nonlinear switched model to take into account not only the nonlinear nature but especially also the intrinsic discontinuity of the gear-shifting process. Then, a new nonlinear switched observer is proposed to *simultaneously* estimate the nonlinear dynamics, thus the shaft torque, and the unknown resistance torque for IMT systems. Motivated by the observer structure in [26], the proposed observer design does not require any specific matching condition as for decoupling-based UIO design [13], [27]–[30], nor *a priori* information about the unknown resistance torque as for proportional-integral observer design [31].

Considering the class of amplitude-bounded sensor noises and disturbances, practically encountered in IMT applications, their effects are minimized via an $\ell_\infty-$gain performance, *i.e.*, peak-to-peak disturbance attenuation. Using Lyapunov stability theory, sufficient conditions are derived to design a nonlinear switched observer with a guaranteed $\ell_\infty-$gain for disturbance attenuation and a decay rate for a specified closed-loop convergence. The observer design is recast as a convex optimization problem under linear matrix inequality (LMI) constraints, which can be effectively solved using semidefinite programming techniques [25]. In particular, the negative impacts of expressive discontinuities at switching instants can be mitigated via an additional bumps limitation constraint, expressed in terms of LMIs, which can be directly incorporated into the optimization-based observer design problem. Hence, the gear-shifting impact under the effect of high-frequency sensor noises and disturbances can be minimized for the estimation of IMT nonlinear dynamics and unknown resistance torque. Specifically, the contributions of this paper can be summarized as follows.

- A simple nonlinear observer is proposed to *jointly* estimate the shaft torque and the unknown resistance torque of IMT systems. The switching nature of IMT dynamics is explicitly considered in the observer design.
- The proposed observer design does not require any specific matching condition nor *a priori* information on the resistance torque. The UIO design methods in [13], [27]–[30] and their direct extensions cannot be applied to the considered IMT system due to such a matching condition.
- Conditions for ℓ_∞ observer design and for smoothness guarantee at switching instants are expressed as LMI constraints to facilitate the design procedure. Comparative results, obtained under various operating conditions, show the practical relevance of the proposed estimation method.

The paper is organized as follows. Section II describes the nonlinear dynamics of IMT powertrain systems. Section III first formulates the estimation problem before providing LMI conditions for ℓ_∞ nonlinear switched observer design. The guarantee on the bumps limitation to mitigate the random switching effect of gear-shifting is also discussed. Illustrative results and comparative studies are presented in Section IV. Section V provides concluding remarks and future works.

Notation. We denote $\mathbb{N}_+$ the set of positive integers, $\mathbb{R}$ the set of real numbers, $\mathbb{R}_+$ the set of positive real numbers, and $\mathcal{I}_q = \{1,\dots,q\} \subset \mathbb{N}_+$. For a vector a, its jth element is denoted by a_j, $\|a\|$ denotes the 2-norm of a, *i.e.*, $\|a\| = \sqrt{a^\top a}$. For a matrix Y, its transpose is denoted by $Y^\top$, $Y \succ 0$ ($Y \prec 0$) means that Y is positive (negative) definite, and $\mathrm{He}Y = Y + Y^\top$. For any bounded function $f(\cdot) : \mathbb{R} \to \mathbb{R}^n$, we define $\|f(\cdot)\|_\infty = \sup_{t\in\mathbb{R}} \|f(t)\|$ as its ℓ_∞-norm. The symbol $\star$ represents the transposed terms in a symmetric matrix. For two vectors $x, y \in \mathbb{R}^n$, we denote $\mathrm{co}(x,y) = \{(1-\lambda)x+\chi y : \ \lambda \in [0,1]\}$ as the convex hull of x and y. For $b \in \mathcal{I}_l$, denote $\zeta_l(b) = [0,\dots,0,1_{b^{\text{th}}},0,\dots,0]^\top \in \mathbb{R}^l$ as the canonical basis of $\mathbb{R}^l$. Denote I as the unit matrix, $\lambda_{\max}(X)$ and $\lambda_{\min}(X)$ as the maximum and minimum eigenvalues of a real symmetric matrix X, respectively. We omit the function arguments when the meaning is clear.

II. Description of IMT Powertrain Dynamics

We consider an IMT powertrain system, depicted in Fig. 1, which consists of a differential system, a two-speed clutchless automated manual transmission system and an electric driving motor. The system parameters are given in Table I. The IMT powertrain dynamics can be described by [8]

$$\begin{aligned} J_{in}\dot{\omega}_{in} &= T_m - T_t - c_m\omega_m \\ J_{os}\dot{\omega}_{out} &= i_{g\eta}T_t - \frac{T_s}{i_f} \\ J_v\dot{\omega}_w &= T_s - T_L \end{aligned} \tag{1}$$

where ω_{out} is the transmission output shaft speed, ω_{in} is the transmission input shaft speed, ω_w is the wheel speed, ω_m is

the motor speed, T_m is the motor torque, T_t is the synchronizer torque, and $\eta \in \{1, 2\}$ represents the current gear stage. The equivalent inertia of the transmission input shaft J_{in} and the drive shaft J_v are defined as

$$J_{in} = J_m + J_{is} + \frac{J_{cs}}{i_g^2} + \frac{J_{gh}}{i_g^2 i_{gh}^2} + \frac{J_{gl}}{i_g^2 i_{gl}^2}$$
$$J_v = J_w + m_v r_w^2.$$

The drive shaft torque T_s can be expressed as

$$T_s = k_s \theta_s + c_s \left(\frac{\omega_m}{i_{g\eta} i_f} - \omega_w \right) \tag{2}$$

where the shaft torsion angle of the drive shaft is given by

$$\theta_s = \frac{\theta_m}{i_{g\eta} i_f} - \theta_w, \quad \eta \in \{1, 2\} \tag{3}$$

with $i_{g1} = i_g i_{gl}$ and $i_{g2} = i_g i_{gh}$. The torque of the external resistance loads is expressed as

$$T_L = T_d + T_a \tag{4}$$

where T_d represents the lumped torque stemmed from the rolling resistance and the road gradient effect, which cannot be measured or accurately modeled. The air drag torque T_a can be expressed as

$$T_a = 0.5 \rho_{air} A_f C_d v^2 r_w \tag{5}$$

where v is the vehicle speed. Without considering the wheel slip, the vehicle speed can be determined as $v = \omega_w r_w$. Hence, we can rewrite the air drag torque T_a in (5) as

$$T_a = f(\omega_w) \omega_w \tag{6}$$

with $f(\omega_w) = 0.5 \rho_{air} A_f C_d r_w^3 \omega_w$.

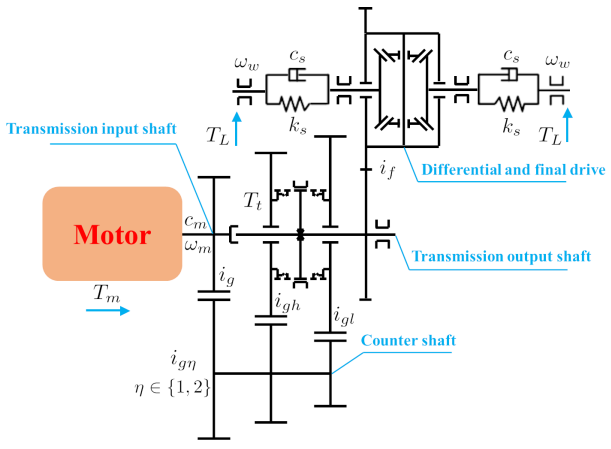

Fig. 1: Schematic of a two-speed integrated motor-transmission powertrain system.

Remark 1. Note from expressions (2) and (3) that the nonlinear dynamics of system (1) depends on the selected current gear stage η. Then, the nonlinear IMT model (1) can be considered as a switched system, where the gear switching signal η is governed by a gear shifting supervisor according to the driver intention [32].

TABLE I: IMT system parameters.

Parameter	Description	Value
J_m	Motor inertia	0.11 [kgm^2]
J_{gh}	High speed gear inertia	0.0409 [kgm^2]
J_{gl}	Low speed gear inertia	0.0194 [kgm^2]
J_{is}	Transmission input shaft inertia	0.0172 [kgm^2]
J_{cs}	Transmission counter shaft inertia	0.0923 [kgm^2]
J_{os}	Transmission output shaft inertia	0.293 [kgm^2]
J_w	Wheel inertia	1.7747 [kgm^2]
m_v	Vehicle mass	1463 [kg]
r_w	Wheel radius	0.3 [m]
k_s	Shaft spring constant	9520 [Nm/rad]
c_s	Shaft damping constant	59 [Nm,s/rad]
i_g	Ratio of input shaft and counter shaft	2.21
i_{gl}	Ratio of counter shaft and 1st gearwheel	0.45
i_{gh}	Ratio of counter shaft and 2nd gearwheel	0.69
i_f	Final reduction gear ratio	3.667
ρ_{air}	Air density	1.29 [kgm^3]
C_d	Aerodynamic drag constant	0.325
A_f	Effective front area	1.8 [m^2]
g	Gravitational acceleration	9.8 [m/s^2]
μ	Tire rolling resistance constant	0.01 [Nms/rad]
c_m	Motor damping	0.01 [Nms/rad]

The angular rotation speed of the transmission input shaft ω_{in} is generally very close to the angular rotation speed of the motor ω_m. Moreover, the transmission output shaft speed ω_{out} is proportional to the transmission input shaft speed ω_{in}. Hence, the dynamics of the motor and the transmission system can be simplified as

$$J_\eta \dot{\omega}_{in} = T_m - \frac{T_s}{i_{g\eta} i_f} - c_m \omega_m \tag{7}$$

with $J_\eta = J_{in} + \frac{J_{os}}{i_{g\eta}^2 i_f^2}$ and $\eta \in \{1, 2\}$. From (2), (4), (6) and (7), the nonlinear dynamics of the IMT system (1) can be represented in the following state-space form:

$$\dot{x} = A_\eta x + B_\eta u + D d + G \phi(x), \quad \eta \in \{1, 2\} \tag{8}$$

where $\phi(x) = \omega_w^2$, $x = \begin{bmatrix} \omega_m & \theta_s & \omega_w \end{bmatrix}^\top$ is the state vector, $u = T_m$ is the *known* input, and $d = T_d$ is the *unknown* input. The state-space matrices of the IMT system (8) are given by

$$A_\eta = \begin{bmatrix} -\frac{c_m i_{g\eta}^2 i_f^2 + c_s}{J_\eta i_{g\eta}^2 i_f^2} & -\frac{k_s}{J_\eta i_{g\eta} i_f} & \frac{c_s}{J_\eta i_{g\eta} i_f} \\ \frac{1}{i_{g\eta} i_f} & 0 & -1 \\ \frac{c_s}{J_v i_{g\eta} i_f} & \frac{k_s}{J_v} & -\frac{c_s}{J_v} \end{bmatrix}$$
$$B_\eta = \begin{bmatrix} \frac{1}{J_\eta} \\ 0 \\ 0 \end{bmatrix}, \quad D = \begin{bmatrix} 0 \\ 0 \\ -\frac{1}{J_v} \end{bmatrix}, \quad G = \begin{bmatrix} 0 \\ 0 \\ -\frac{0.5 \rho_{air} A_f C_d r_w^3}{J_v} \end{bmatrix}.$$

For normal operating conditions, the IMT system states are bounded within a compact set $x \in \mathscr{B}_x$, defined as

$$\mathscr{B}_x = \left\{ \omega_m \in [\underline{\omega}_m, \overline{\omega}_m],\ \theta_s \in [\underline{\theta}_s, \overline{\theta}_s],\ \omega_w \in [\underline{\omega}_w, \overline{\omega}_w] \right\}$$

where $\underline{\omega}_m = 0$ [rpm], $\overline{\omega}_m = 1000$ [rpm], $\underline{\theta}_s = -0.5$ [rad] and $\overline{\theta}_s = 1$ [rad], and $\underline{\omega}_w = 0$ [rpm], $\overline{\omega}_w = 250$ [rpm]. Note that the motor rotation speed ω_m can be obtained from the motor control unit. However, the measurements of the shaft torsion angle θ_s and the wheel rotation speed ω_w are not available in practice due to sensor costs. Moreover, with low-cost sensors,

the undesired effects of measurement noises are unavoidable. Hence, the output equation of system (8) is defined as

$$y = Cx + f,$$

where $C = \begin{bmatrix} 1 & 0 & 0 \end{bmatrix}$, and f is the measurement noise.

By the flexible shaft theory, estimating the shaft torque T_s can be converted into an estimation problem of the shaft torsion angle θ_s. Moreover, the information of the resistance torque T_d is important for estimation and control design of IMT powertrain systems. Hence, this paper aims at providing an effective algorithm to simultaneously estimate both the state x and the unknown input d of the IMT system (7). This estimation algorithm is based on a nonlinear switched observer (NSO), whose structure is depicted in Fig. 2. A numerically tractable NSO design is discussed in the next section.

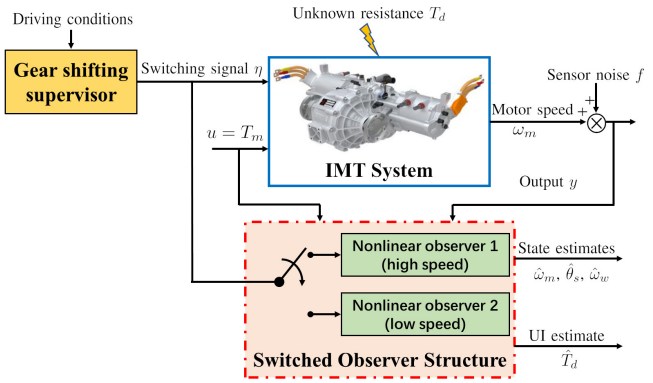

Fig. 2: Structure of the proposed nonlinear switched observer.

III. Nonlinear Switched Observer Design With Smoothness Guarantee

This section first describes the general class of nonlinear switched systems to be considered. Then, the related ℓ_∞ nonlinear switched observer design problem is formulated.

A. Problem Formulation

For generality of the proposed estimation method, we consider a more general form of system (8) as

$$\begin{aligned} \dot{x} &= A_\eta x + B_\eta u + D_\eta d + G_\eta \phi(x) \\ y &= C_\eta x + F_\eta f \end{aligned} \tag{9}$$

where $u \in \mathbb{R}^{n_u}$ is the known input, $x \in \mathscr{B}_x \subseteq \mathbb{R}^{n_x}$ is the system state, $f \in \mathbb{R}^{n_f}$ is the measurement noise, $y \in \mathbb{R}^{n_y}$ is the measured output, $d \in \mathbb{R}^{n_d}$ is the unknown input (UI), $\eta : \mathbb{R}_+ \to \mathcal{I}_N$ is a switching signal that selects a particular subsystem, at each instant of time, among N available ones defined by

$$\mathscr{C}_i = \begin{bmatrix} A_i & B_i & D_i & G_i & 0 \\ C_i & 0 & 0 & 0 & F_i \end{bmatrix}, \quad i \in \mathcal{I}_N.$$

We say that $i \in \mathcal{I}_N$ is the active subsystem at time t if $\eta(t) = i$. Since the switching rule is governed by a supervisor, we assume that $\eta(t)$ is unknown *a prior*, but its instantaneous value is available in real time. The nonlinear function $\phi(x) : \mathscr{B}_x \to \mathbb{R}^{n_\phi}$ is differentiable with respect to the state x, whose elements cannot be measured from the output y. For observer design, we assume that the pairs (A_i, C_i), for $i \in \mathcal{I}_N$, are observable. Moreover, the following assumptions are also considered for the nonlinear switched system (9).

Assumption 1. The matrices D_i, for $i \in \mathcal{I}_N$, are of full column rank, *i.e.*, $\mathrm{rank}(D_i) = n_d$.

Remark 2. Assumption 1 does not imply any loss of generality since it can be achieved by removing redundant components of d. In contrast to most of existing UIO design results [13], [27], [29], [33], the well-known matching condition, *i.e.*, $\mathrm{rank}(C_i D_i) = \mathrm{rank}(D_i)$, for $\forall i \in \mathcal{I}_N$, is not necessary in this work. It is important to note that the IMT system (8) does not verify such a matching condition, thus classical UIO observer design is unapplicable to this system.

Assumption 2. The unmeasured function $\phi(x)$ satisfies the following boundedness condition:

$$\underline{\varrho}_{ij} \leq \frac{\partial \phi_i}{\partial x_j}(x) \leq \overline{\varrho}_{ij}, \qquad x \in \mathscr{B}_x \tag{10}$$

for $\forall (i,j) \in \mathcal{I}_{n_\phi} \times \mathcal{I}_{n_x}$, with

$$\underline{\varrho}_{ij} = \min_{\varrho \in \mathscr{B}_x} \left(\frac{\partial \phi_i}{\partial x_j}(\varrho) \right), \quad \overline{\varrho}_{ij} = \max_{\varrho \in \mathscr{B}_x} \left(\frac{\partial \phi_i}{\partial x_j}(\varrho) \right).$$

Remark 3. Assumption 2 is not restrictive since for normal operating conditions of any engineering systems, the state x is always physically bounded, *i.e.*, $x \in \mathscr{B}_x$. Hence, from the mathematical expression of function $\phi(x)$, the bounds $\underline{\varrho}_{ij}$ and $\overline{\varrho}_{ij}$ in (10) can be directly computed. For instance, with the IMT system (8), we have $\phi(x) = \omega_w^2 = x_3^2$. Then, it follows that $2\underline{\omega}_w \leq \frac{\partial \phi}{\partial x_3}(x) = 2\omega_w \leq 2\overline{\omega}_w$.

Assumption 3. The measurement noise $f(t)$ and the time derivative of the unknown input $d(t)$ are assumed to be bounded, *i.e.*, $\|f(t)\| \leq \theta_1$ and $\|\dot{d}(t)\| \leq \theta_2$, for some positive scalars θ_1 and θ_2.

Remark 4. The boundedness condition in Assumption 3 is less restrictive than that in [34], where both $d(t)$ and $\|\dot{d}(t)\|$ are required to be bounded. Moreover, the exact bound values θ_1 and θ_2 are not required for the observer design conditions. In particular, no *a priori* information on the unknown input $d(t)$ is required as for proportional-integral observer design, see [31], [35], [36] and related references. Note that for the IMT system (8), the unknown input $d(t)$ is related to the resistance torque and $f(t)$ is the sensor noise, for which this assumption is practically reasonable.

To avoid the necessity of the observer matching condition for simultaneous estimation of the state x and the unknown input d, we consider the following observer structure:

$$\begin{aligned} \dot{\hat{x}} &= A_\eta \hat{x} + B_\eta u + D_\eta \hat{d} + G_\eta \phi(\hat{x}) + L_\eta (y - \hat{y}) \\ \dot{\hat{z}} &= -K_\eta D_\eta \hat{z} - K_\eta \left(A_\eta \hat{x} + B_\eta u + G_\eta \phi(\hat{x}) + D_\eta K_\eta \hat{x} \right) \\ \hat{y} &= C_\eta \hat{x} \\ \hat{d} &= \hat{z} + K_\eta \hat{x} \end{aligned} \tag{11}$$

where $\hat{x}$ is the estimate of x, $\hat{y}$ is the estimate of y, $\hat{d}$ is the estimate of d, and $\hat{z}$ is the estimate of the intermediate variable z, defined as

$$z = d - K_\eta x. \tag{12}$$

For observer design, the gain matrix K_η is selected as

$$K_\eta = \tau D_\eta^\top \tag{13}$$

where τ is a positive scalar. The observer gain $L_\eta \in \mathbb{R}^{n_x \times n_y}$ is to be determined. Let us define the estimation errors as

$$e_x = x - \hat{x}, \quad e_z = z - \hat{z}, \quad e_d = d - \hat{d}. \tag{14}$$

It follows from (12) and (13) that

$$d = z + K_\eta x. \tag{15}$$

Then, the UI estimation error can be defined from (11), (14) and (15) as

$$e_d = e_z + K_\eta e_x. \tag{16}$$

As a result, the dynamics of the estimation errors can be obtained from (9), (11) and (16) as

$$\begin{aligned} \dot{e}_x &= (A_\eta - L_\eta C_\eta)e_x + G_\eta \delta_\phi + D_\eta(e_z + K_\eta e_x) - L_\eta F_\eta f \\ \dot{e}_z &= \dot{d} - K_\eta(A_\eta + D_\eta K_\eta)e_x - K_\eta G_\eta \delta_\phi - K_\eta D_\eta e_z \end{aligned} \tag{17}$$

with $\delta_\phi = \phi(x) - \phi(\hat{x})$. The following mean value theorem is useful to reformulate the mismatching nonlinear term δ_ϕ as a function of e_x for nonlinear observer design.

Lemma 1 ([21])**.** For any nonlinear function $\phi(x) : \mathbb{R}^{n_x} \to \mathbb{R}^{n_\phi}$, differentiable on $\mathrm{co}(\alpha, \beta)$, there exist constant vectors $\gamma_i \in \mathrm{co}(\alpha, \beta)$, $\gamma_i \neq \alpha$, $\gamma_i \neq \beta$, for $i \in \mathcal{I}_{n_\phi}$, such that

$$\phi(\alpha) - \phi(\beta) = \left(\sum_{i=1}^{n_\phi} \sum_{j=1}^{n_x} \zeta_{n_\phi}(i) \zeta_{n_x}^\top(j) \frac{\partial \phi_i}{\partial x_j}(\gamma_i) \right) (\alpha - \beta).$$

Applying Lemma 1 to function $\phi(x)$, the mismatching nonlinear term δ_ϕ can be reformulated as

$$\begin{aligned} \delta_\phi &= \left(\sum_{i=1}^{n_\phi} \sum_{j=1}^{n_x} \zeta_{n_\phi}(i) \zeta_{n_x}^\top(j) \frac{\partial \phi_i}{\partial x_j}(\vartheta) \right) (x - \hat{x}) \\ &= \Phi(\vartheta) e_x \end{aligned} \tag{18}$$

for $\vartheta \in \mathrm{co}(x, \hat{x})$. Considering Assumption 2, the parameters $\rho_{ij} = \frac{\partial \phi_i}{\partial x_j}(\vartheta)$, for $i \in \mathcal{I}_{n_\phi}$ and $j \in \mathcal{I}_{n_x}$, are unknown but bounded. Then, the elements of the unknown matrix $\Phi(\vartheta)$ belong to a bounded convex set $\mathscr{S}_\phi$, defined as

$$\mathscr{S}_\phi = \left\{ \Phi(\vartheta) : \ \frac{\partial \phi_i}{\partial x_j}(\cdot) \in \{\underline{\varrho}_{ij}, \overline{\varrho}_{ij}\} \right\}, \quad (i,j) \in \mathcal{I}_{n_\phi} \times \mathcal{I}_{n_x}$$

where $\underline{\varrho}_{ij}$ and $\overline{\varrho}_{ij}$ are given in (10). From (13), (17) and (18), the state estimation error dynamics can be rewritten as

$$\dot{\bar{e}} = \begin{bmatrix} A_{11} & A_{12} \\ A_{21} & A_{22} \end{bmatrix} \bar{e} + \begin{bmatrix} -L_\eta F_\eta & 0 \\ 0 & I \end{bmatrix} w \tag{19}$$

with $\bar{e} = \begin{bmatrix} e_x^\top & e_z^\top \end{bmatrix}^\top$, $w = \begin{bmatrix} f^\top & \dot{d}^\top \end{bmatrix}^\top$, and

$$\begin{aligned} &A_{11} = \mathscr{A}_\eta(\vartheta) - L_\eta C_\eta + \tau D_\eta D_\eta^\top, \qquad A_{12} = D_\eta \\ &A_{21} = -\tau D_\eta^\top \mathscr{A}_\eta(\vartheta) - \tau^2 D_\eta^\top D_\eta D_\eta^\top, \quad A_{22} = -\tau D_\eta^\top D_\eta \\ &\mathscr{A}_\eta(\vartheta) = A_\eta + G_\eta \Phi(\vartheta). \end{aligned}$$

We are now ready to formalize the nonlinear switched observer design problem for system (9).

Problem 1. Consider the nonlinear switched system (9) and the observer structure (11) with K_η given in (13). Determine the observer gain matrices of appropriate dimensions L_i, for $i \in \mathcal{I}_N$, such that the estimation error dynamics (19) satisfies the following specifications.

- If $w(t) = 0$, for $\forall t \in \mathbb{R}_+$, the estimation error system (19) is globally exponentially stable.
- If $w(t) \neq 0$, for $\forall t \in \mathbb{R}_+$, for any initial condition $\bar{e}_0$ and any bounded $w(t)$, the estimation error $\bar{e}(t)$ is uniformly ultimately bounded and satisfies the condition

$$\limsup_{t \to \infty} \|\bar{e}(t)\| \leq \psi \|w(t)\|_\infty \tag{20}$$

  where ψ is the $\ell_\infty-$gain performance index.

We remark from (20) that a smaller value of the $\ell_\infty-$gain ψ yields a better estimation performance.

B. LMI-Based Switched Nonlinear Observer Design

The following theorem presents a numerically tractable solution to design a switched nonlinear observer (11) such that the specifications, stated in Problem 1, are verified.

Theorem 1. Consider system (9) and two positive scalars τ and υ. If there exist a positive definite matrix $P \in \mathbb{R}^{n_x \times n_x}$, matrices $H_i \in \mathbb{R}^{n_x \times n_y}$, for $i \in \mathcal{I}_N$, and positive scalars ϵ, ν, φ, such that the following optimization problem is feasible:

$$\begin{aligned} &\textsf{minimize} \qquad \varphi + \nu \\ &\text{subject to} \\ &\mathrm{He} \begin{bmatrix} \Omega_{1i} & \Omega_{2i} & -H_i F_i & 0 \\ 0 & -\tau\epsilon D_i^\top D_i + \upsilon\epsilon I & 0 & \epsilon I \\ 0 & 0 & -\upsilon\nu I & 0 \\ 0 & 0 & 0 & -\upsilon\nu I \end{bmatrix} \prec 0 \end{aligned} \tag{21}$$

$$\begin{bmatrix} \bar{P} & I \\ \star & \varphi I \end{bmatrix} \succeq 0 \tag{22}$$

with

$$\begin{aligned} \bar{P} &= \begin{bmatrix} P & 0 \\ 0 & \epsilon I \end{bmatrix}, \quad \mathscr{A}_i(\vartheta) = A_i + G_i \Phi(\vartheta) \\ \Omega_{1i} &= P\mathscr{A}_i(\vartheta) - H_i C_i + \tau P D_i D_i^\top + \upsilon P \\ \Omega_{2i} &= P D_i - \tau^2 \epsilon D_i D_i^\top D_i - \tau\epsilon \mathscr{A}_i^\top(\vartheta) D_i \end{aligned}$$

for $i \in \mathcal{I}_N$ and $\Phi(\vartheta) \in \mathscr{S}_\phi$. Then, the estimation error $\bar{e}(t)$ of system (19) is uniformly ultimately bounded and verifies the $\ell_\infty-$gain performance (20) under any arbitrary switching signal $\eta(t)$. Moreover, the observer gains are defined as

$$L_i = P^{-1} H_i, \quad i \in \mathcal{I}_N. \tag{23}$$

Proof. For stability analysis of the estimation error dynamics (19), we consider the Lyapunov function

$$V(\bar{e}) = e^\top \bar{P} e. \tag{24}$$

The time derivative of function $V(\bar{e})$ along the trajectory of system (19) is given by

$$\begin{aligned}\dot{V}(\bar{e}) = {} & e_x^\top \left(\mathrm{He}\left[P\left(\mathscr{A}_\eta(\vartheta) - L_\eta C_\eta\right)\right]\right) e_x \\ & - 2\tau\epsilon e_z^\top D_\eta^\top \mathscr{A}_\eta(\vartheta) e_x - 2\tau^2 \epsilon e_z^\top D_\eta^\top D_\eta D_\eta^\top e_x \\ & + 2e_x^\top P D_\eta e_z - 2\tau\epsilon e_z^\top D_\eta^\top D_\eta e_z + 2\epsilon e_z^\top \dot{d} \\ & + 2\tau e_x^\top P D_\eta D_\eta^\top e_x - 2e_x^\top P L_\eta F_\eta f. \end{aligned} \tag{25}$$

Moreover, the satisfaction of condition (21) implies that

$$\mathrm{He}\begin{bmatrix} \Omega_1 & \Omega_2 & -H_\eta F_\eta & 0 \\ 0 & -\tau\epsilon D_\eta^\top D_\eta + \upsilon\epsilon I & 0 & \epsilon I \\ 0 & 0 & -\upsilon\nu I & 0 \\ 0 & 0 & 0 & -\upsilon\nu I \end{bmatrix} \prec 0 \tag{26}$$

for $\Phi(\vartheta) \in \mathscr{S}_\phi$, with

$$\begin{aligned}\Omega_1 &= P\mathscr{A}_\eta(\vartheta) - H_\eta C_\eta + \tau P D_\eta D_\eta^\top + \upsilon P \\ \Omega_2 &= P D_\eta - \tau^2 \epsilon D_\eta D_\eta^\top D_\eta - \tau\epsilon \mathscr{A}_\eta^\top(\vartheta) D_\eta.\end{aligned}$$

Pre- and post-multiplying (26) with $\begin{bmatrix} e_x^\top & e_z^\top & f^\top & \dot{d}^\top \end{bmatrix}$ and its transpose, we can obtain the following condition after some algebraic manipulations:

$$\dot{V}(\bar{e}) \le 2\upsilon\left(\nu\|w\|^2 - V(\bar{e})\right) \tag{27}$$

where $V(\bar{e})$ and $\dot{V}(\bar{e})$ are given in (24) and (25), respectively. Note that inequality (27) implies that

$$\dot{V}(\bar{e}) \le 2\upsilon\left(\nu\|w\|_\infty^2 - V(\bar{e})\right). \tag{28}$$

Multiplying the left and right sides of (28) by $e^{2\upsilon t}$, and then integrating over the time interval $[t_0, t]$, we have

$$\begin{aligned} e^{2\upsilon t} V(\bar{e}) &\le e^{2\upsilon t_0} V(\bar{e}_0) + 2\upsilon\nu\|w\|_\infty^2 \int_{t_0}^{t} e^{2\upsilon\varpi} d\varpi \\ &= e^{2\upsilon t_0} V(\bar{e}_0) + \nu\|w\|_\infty^2 (e^{2\upsilon t} - e^{2\upsilon t_0}). \end{aligned} \tag{29}$$

It follows from (29) that

$$\begin{aligned} V(\bar{e}) &\le \nu\|w\|_\infty^2 \left(1 - e^{-2\upsilon(t-t_0)}\right) + e^{-2\upsilon(t-t_0)} V(\bar{e}_0) \\ &\le \nu\|w\|_\infty^2 + e^{-2\upsilon(t-t_0)} V(\bar{e}_0). \end{aligned} \tag{30}$$

Moreover, from (24), one has

$$\sigma_1\|\bar{e}\|^2 \le V(\bar{e}) \le \sigma_2\|\bar{e}\|^2 \tag{31}$$

with $\sigma_1 = \min[\lambda_{\min}(P), \epsilon]$ and $\sigma_2 = \max[\lambda_{\max}(P), \epsilon]$. Hence, it follows from (30) and (31) that

$$\sigma_1\|\bar{e}\|^2 \le \sigma_2 e^{-2\upsilon(t-t_0)}\|\bar{e}_0\|^2 + \nu\|w\|_\infty^2$$

which implies that

$$\|\bar{e}\| \le \sqrt{\frac{\sigma_2}{\sigma_1}} e^{-\upsilon(t-t_0)}\|\bar{e}_0\|^2 + \sqrt{\frac{\nu}{\sigma_1}}\|w\|_\infty. \tag{32}$$

For any bounded $w(t)$ and any initial condition $\bar{e}_0$, it follows from (32) that the estimation error $\bar{e}(t)$ is globally bounded. In addition, if $w(t) = 0$, the estimation error dynamics (19) is exponentially stable.

Applying the Schur complement lemma [25], condition (22) can be shown to be equivalent to

$$\bar{P} - \varphi^{-1} I \succeq 0. \tag{33}$$

Pre- and post-multiplying (33) with $\bar{e}^\top$ and $\bar{e}$, it follows that

$$\|\bar{e}\|^2 \le \varphi V(\bar{e}). \tag{34}$$

From (30) and (34), we have

$$\|\bar{e}\|^2 \le \sqrt{\varphi V(\bar{e}_0)} e^{-\upsilon(t-t_0)} + \sqrt{\nu\varphi}\|w\|_\infty. \tag{35}$$

For any bounded $w(t)$ and any initial condition $\bar{e}_0$, it follows from (35) that

$$\limsup_{t\to\infty} \|e\| \le \psi\|w\|_\infty$$

with $\psi = \sqrt{\nu\varphi}$. The proof can be now concluded. □

Remark 5. To further reduce the observer design conservatism, a free decision variable K_η can be considered for the optimization problem in Theorem 1. However, this choice leads to a non-convex observer design formulation with bilinear matrix inequality (BMI) constraints, which significantly induces numerical difficulties in finding suitable observer gains for practical uses. To avoid this issue, we select the matrix gain K_η of the specific form (13). Note from (16) that the gain factor τ offers a degree of freedom for the matrix gain K_η to improve the correction of the UI estimation error.

C. Smoothness Guarantee Constraints

Expressive discontinuities at switching instants often arise within the context of switched systems [37]. This can significantly deteriorate the practical estimation performance of switched systems. To deal with this major issue, this section provides numerically tractable conditions to limit the amplitude of these discontinuities, thus to guarantee the smoothness at switching instants. The proposed solution is motivated by the control bumps limitation for switched linear control design in [38]. To this end, we impose the following bumps limitation constraint (BLC) on the observer gain matrices:

$$\|L^* - L_i\| < \kappa, \quad i \in \mathcal{I}_N \tag{36}$$

where the constant matrix $L^* \in \mathbb{R}^{n_x \times n_y}$ and the positive scalar κ are to be determined.

Remark 6. Condition (36) aims at selecting among the optimal observers, designed by Theorem 1, the one yielding limited discontinuities at the switching instants. Indeed, all the observer gains L_i, for $i \in \mathcal{I}_N$, are constrained to be "close" enough to the constant matrix L^* with an amplitude error, specified by κ. As illustrated in Section IV, this smoothness constraint is particularly important to guarantee an acceptable estimation performance in the presence of disturbances/noises.

The additional BLC condition (36) can be expressed in terms of LMIs as shown in the following theorem.

Theorem 2. If there exist positive scalars β and γ, a positive definite matrix $P \in \mathbb{R}^{n_x \times n_x}$, and matrices $L^*, H_i \in \mathbb{R}^{n_x \times n_y}$, for $i \in \mathcal{I}_N$, such that

$$\begin{bmatrix} \beta I & L^* & I \\ \star & \gamma I & H_i^\top \\ \star & \star & P \end{bmatrix} \succ 0, \quad i \in \mathcal{I}_N. \tag{37}$$

Then, the observer gain matrices L_i defined in (23), for $i \in \mathcal{I}_N$, satisfy constraint (36) with $\kappa = \sqrt{\beta\gamma}$.

Proof. Applying Schur complement lemma to (37), this condition is equivalent to

$$\begin{bmatrix} \beta I & L^* \\ \star & \gamma I \end{bmatrix} - \begin{bmatrix} I \\ H_i^\top \end{bmatrix} P^{-1} \begin{bmatrix} I & H_i \end{bmatrix} \succ 0. \tag{38}$$

Condition (38) can be rewritten as

$$\begin{bmatrix} \beta I & L^* - P^{-1}H_i \\ \star & \gamma I \end{bmatrix} - \underbrace{\begin{bmatrix} P^{-1} & 0 \\ 0 & H_i^\top P^{-1} H_i \end{bmatrix}}_{\Upsilon_i} \succ 0. \tag{39}$$

Since $P \succ 0$, one has $\Upsilon_i \succ 0$. Hence, condition (39) yields

$$\begin{bmatrix} \beta I & L^* - P^{-1}H_i \\ \star & \gamma I \end{bmatrix} \succ 0. \tag{40}$$

Using expression (23), we can directly obtain (36) from (40) with $\kappa = \sqrt{\beta\gamma}$. This completes the proof. □

The bumps limitation constraint (37) can be incorporated in the observer design conditions in Theorem 1. Algorithm 1 summarizes the procedure to design a nonlinear switched observer with smoothness guarantee.

Algorithm 1: Observer Design Procedure

Input: Nonlinear switched system (9)
Output: Nonlinear switched observer (11)
1 Select a positive scalar τ
2 Compute K_η from (13)
3 Compute P and H_i, for $i \in \mathcal{I}_N$, by solving LMI conditions in Theorems 1 and 2
4 Compute L_i, for $i \in \mathcal{I}_N$, from (23)
5 Compute L_η and construct observer (11)

Remark 7. Larger values of the gain factor τ in (13) and the decay rate υ in the Lyapunov condition (27) yield a faster estimation convergence. However, this may induce aggressive estimation behaviors, *e.g.*, estimations with a large overshoot and/or sensitive to noise effects. Hence, these design parameters should be chosen so that the nonlinear observer obtained from Theorems 1 and 2 can avoid these practical issues.

Remark 8. The sufficient design conditions in Theorems 1 and 2 are expressed in terms of LMI constraints, which can be effectively solved using semidefinite programming techniques. In this paper, all the LMI-based design conditions are solved with YALMIP toolbox using SDPT3 solver [39].

IV. Illustrative Results and Evaluations

This section illustrates the effectiveness of the proposed method to simultaneously estimate the state and the unknown input of the IMT system (8). For the observer gain in (13), we select $\tau = 90000$, which leads to $K = \begin{bmatrix} 0 & 0 & -674.4367 \end{bmatrix}$, see Remark 7. A decay rate $\upsilon = 5$ is chosen by trial and error method to guarantee a good estimation convergence under the effect of measurement noises. Solving the design conditions in Theorems 1 and 2, we obtain a switched nonlinear observer (11) while guaranteeing the switching smoothness with

$$L_1 = \begin{bmatrix} 133.882 \\ -0.312 \\ 8.911 \end{bmatrix}, \; L_2 = \begin{bmatrix} 138.375 \\ -0.331 \\ 9.172 \end{bmatrix}, \; L^* = \begin{bmatrix} 87.027 \\ -0.623 \\ 6.868 \end{bmatrix} \tag{41}$$

We also design a nonlinear observer (11) without considering the bumps limitation constraint in Theorem 2. To this end, solving LMI conditions in Theorem 1, we obtain

$$L_1 = \begin{bmatrix} 9359.244 \\ -49.932 \\ 707.934 \end{bmatrix}, \quad L_2 = \begin{bmatrix} 9373.644 \\ -48.674 \\ 687.107 \end{bmatrix}. \tag{42}$$

For comparison purposes, we consider the three following estimation methods.

- NSO-BLC observer, designed with LMI conditions in Theorems 1 and 2.
- NSO-noBLC observer, designed with only LMI conditions in Theorems 1.
- Reduced-order TS fuzzy observer (ROO) proposed in [8]. Note that this observer cannot estimate the unknown resistance torque T_d as NSO-BLC and NSO-noBLC.

For illustrations, we consider that the unknown external load T_d is composed of the rolling resistance torque T_r and the road gradient torque T_g, *i.e.*, $T_d = T_r + T_g$, with

$$T_r = \mu m_v g \cos(\alpha) r_w, \quad T_g = m_v g \sin(\alpha) r_w$$

where α is the road slope angle. Moreover, the test scenarios are performed with the motor torque T_m depicted in Fig. 3, which includes both typical tip-in and tip-out tests.

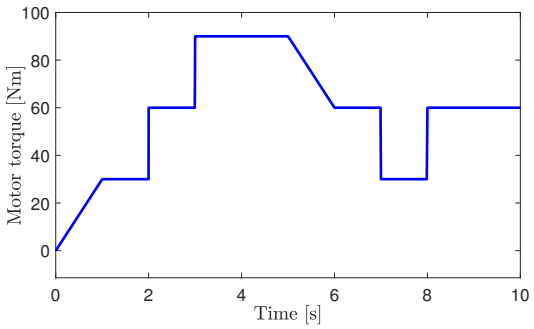

Fig. 3: Profile of the known motor torque input T_m.

A. Scenario 1: Low-High-Low Speed Gear-Shift

For this test scenario, the IMT system initially operates at the low-speed gear. Then, the gear-shifting occurs at 3 [s] and 6 [s] as shown in Fig. 4(a). Fig. 4(b) depicts the measurement

of the motor rotation speed ω_m, which is corrupted by the sensor noise given in Fig. 4(c). Note that we consider here a white noise $f(t)$ with an amplitude less than 1% of the system output $y(t)$, which is reasonable in practice. The profile of the road slope α in this test is shown in Fig. 5, which includes both downhill and uphill driving situations. The initial torsion angle is 0.035 [rad], and the initial motor speed is 0 [rpm], and the initial wheel rotation speed is 43.5 [rpm].

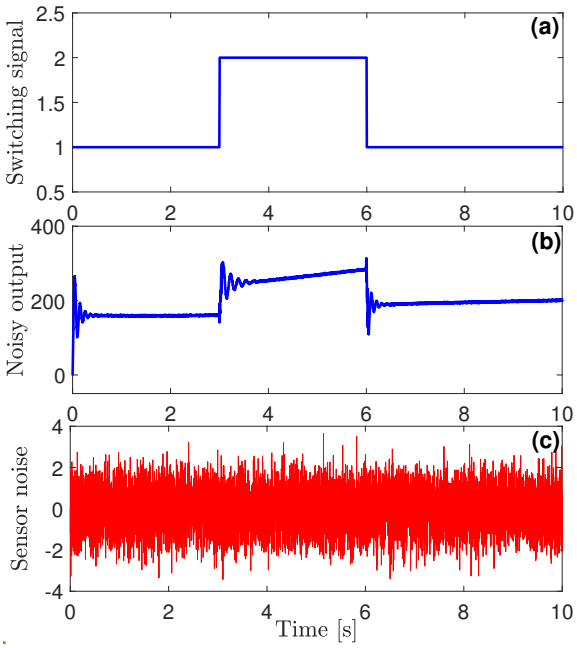

Fig. 4: Scenario 1. (a) switching signal η, (b) noisy output y, (c) sensor noise f.

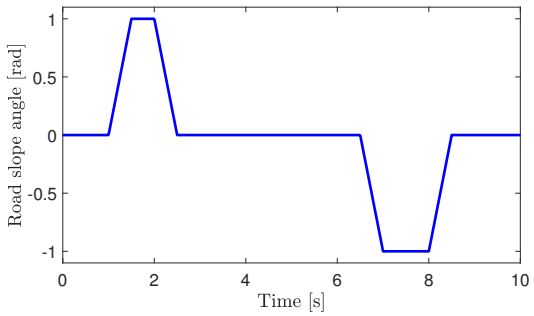

Fig. 5: Road slope angle α for Scenario 1.

The estimation results of the torsion angle θ_s and the wheel rotation speed ω_w are respectively depicted in Figs. 6 and 7, where a special focus is put on the switching instants. Remark that using the time-derivative of the output $\dot{y}$ in the reduced-order observer structure, the estimation method in [8] is very sensitive to the noise effect, which can be slightly attenuated with the NSO-noBLC observer. In particular, taking into account the smoothness constraint (36) via Theorem 2, the gains of the NSO-BLC observer in (42) are significantly reduced compared to those of the NSO-noBLC observer in (41). As a result, despite the small amplitude of the torsion angle, the NSO-BLC observer can achieve a very accurate estimation performance while being almost insensitive to the sensor noise effect. Fig. 8 presents the estimation result of the unknown input T_d. We can see clearly that the resistance torque T_d is well estimated and the estimation with the NSO-BLC observer is much less sensitive to the noise than that with the NSO-noBLC observer. More specifically, taking into account the smoothness guarantee, the NSO-BLC observer allows to avoid significant bumps stemmed from the gear-shifting under sensor noise effects.

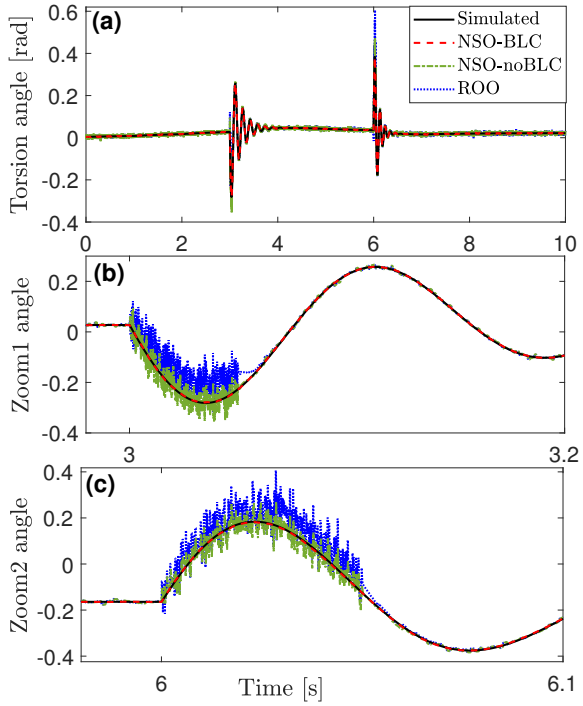

Fig. 6: Scenario 1. (a) estimation of the torsion angle θ_s, (b) zoom at the first gear-shifting, (c) zoom at the second gear-shifting.

For a quantitative performance analysis, we respectively define the mean absolute error (MAE) and the root mean square error (RMSE) as

$$\xi_{\text{MAE}} = \frac{1}{T}\int_0^T \left|\xi(t) - \hat{\xi}(t)\right| dt$$

$$\xi_{\text{RMSE}} = \sqrt{\frac{1}{T}\int_0^T \left(\xi(t) - \hat{\xi}(t)\right)^2 dt}$$

where $\xi(t)$ is the variable of interest, $\hat{\xi}(t)$ is its estimate, and T is the test duration time. The error indicators for the torsion angle θ_s, the wheel rotation speed ω_w and the resistance torque T_d are summarized in Table II. We can see that the proposed method provides more accurate estimation results than the TS fuzzy observer based method in [8]. Moreover, the interest of the bumps limitation constraint is highlighted since all the error indicators of the NSO-BLC observer are clearly smaller than those from the NSO-noBLC observer.

B. Scenario 2: High-Low-High Speed Gear-Shift

For this scenario, the IMT system first operates at the high-speed gear. The gear-shifting profile is depicted in Fig. 9(a).

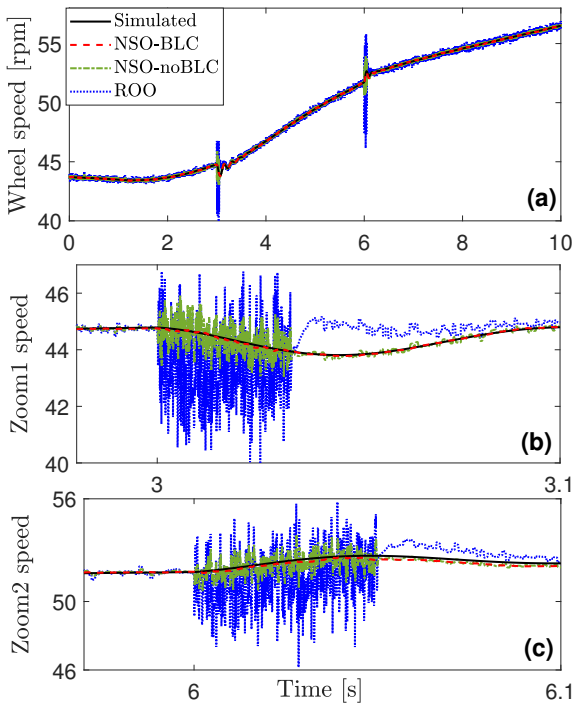

Fig. 7: Scenario 1. (a) estimation of the wheel speed ω_w, (b) zoom at the first gear-shifting, (c) zoom at the second gear-shifting.

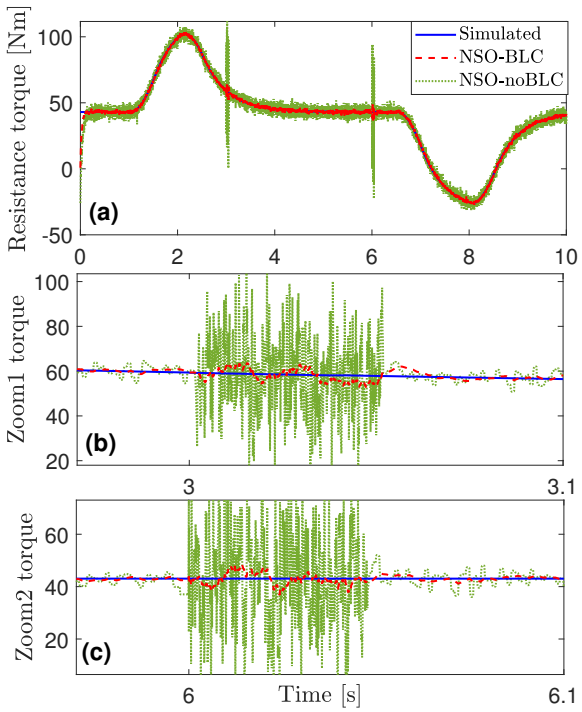

Fig. 8: Scenario 1. (a) estimation of the resistance load torque T_d, (b) zoom at the first gear-shifting, (c) zoom at the second gear-shifting.

The noisy output y the corresponding sensor noise f are shown in Figs. 9(b) and (c), respectively. As the previous scenario, the amplitude of the white noise is also small and less than

TABLE II: Estimation error indicators for Scenario 1.

Error indicator	NSO-BLC	NSO-noBLC	ROO [8]
$\theta_{s\text{MAE}}$ [rad]	0.0005	0.0039	0.0043
$\omega_{w\text{MAE}}$ [rpm]	0.0196	0.0579	0.1248
$T_{d\text{MAE}}$ [Nm]	0.7637	2.3220	–
$\theta_{s\text{RMSE}}$ [rad]	0.0007	0.0059	0.0120
$\omega_{w\text{RMSE}}$ [rpm]	0.0249	0.0838	0.2410
$T_{d\text{RMSE}}$ [Nm]	1.7750	4.1963	–

1% compared to the output amplitude. The road slope profile of this scenario is shown in Fig. 10. The initial torsion angle is 0.001 [rad], the initial motor speed is 0 [rpm], and the initial wheel rotation speed is 56.5 [rpm].

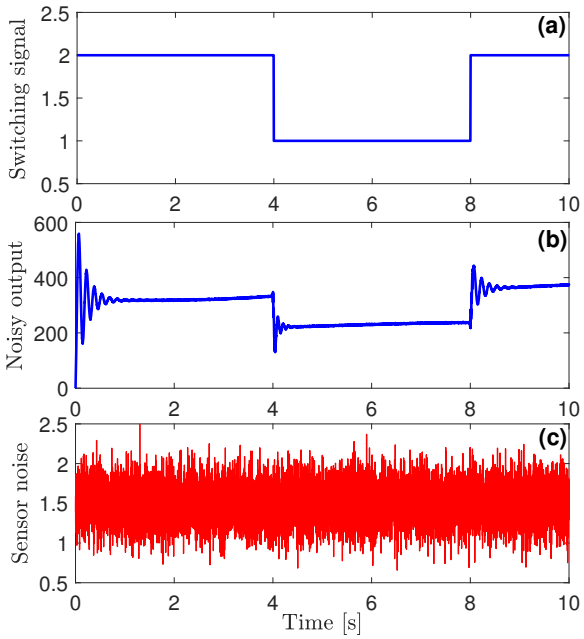

Fig. 9: Scenario 2. (a) switching signal η, (b) noisy output y, (c) sensor noise f.

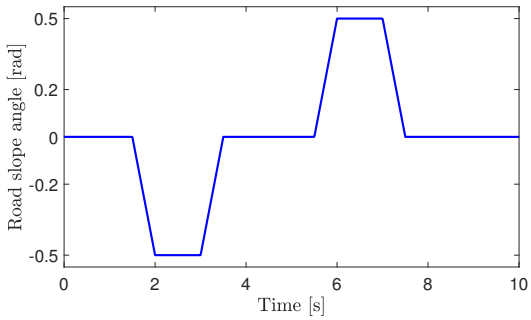

Fig. 10: Road slope angle α for Scenario 2.

The estimation results of the torsion angle θ_s and the wheel rotation speed ω_w are respectively depicted in Figs. 11 and 12, with suitable zooms at the switching instants. We can see that both θ_s and ω_w can be accurately estimated by the proposed NSO-BLC observer under the switching and sensor noise effects. As in Scenario 1, without considering the

bumps limitation in Theorem 2, the estimation performance of the NSO-BLC observer is significantly degraded with the switching occurrences. In particular, under the switching effect, the ROO observer in [8] cannot provide a satisfactory estimation performance, especially for a small-amplitude signal θ_s, compared to NSO-BLC and NSO-noBLC observers due to its high sensitivity to sensor noises. Fig. (13) shows that the unknown resistance torque T_d is well reconstructed by the NSO-BLC observer. Moreover, its estimation is much less sensitive to sensor noises than that provided by the NSO-noBLC observer. Table III summarizes the error indicators obtained with Scenario 2. These indicators quantitatively confirm the estimation performance of the three nonlinear observers and emphasize the practical relevance of the NSO-BLC observer for estimating the IMT powertrain dynamics.

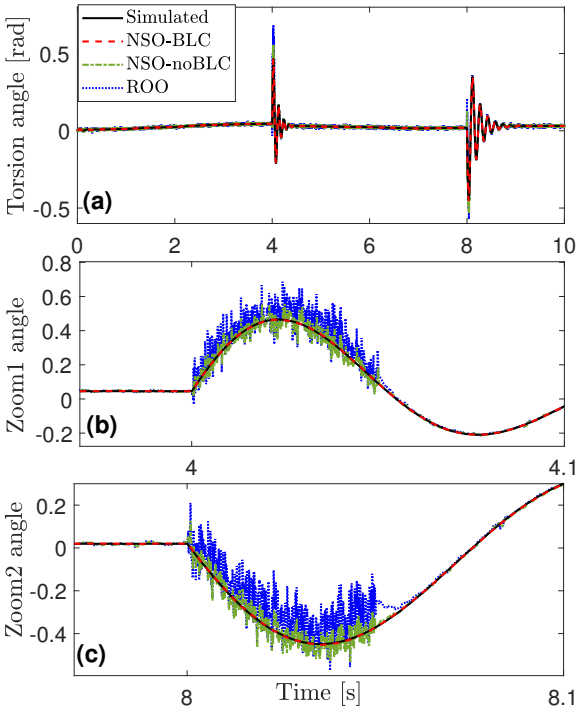

Fig. 11: Scenario 2. (a) estimation of the torsion angle θ_s, (b) zoom at the first gear-shifting, (c) zoom at the second gear-shifting.

TABLE III: Estimation error indicators for Scenario 2.

Error indicator	NSO-BLC	NSO-noBLC	ROO [8]
$\theta_{s\text{MAE}}$ [rad]	0.0005	0.0042	0.0051
$\omega_{w\text{MAE}}$ [rpm]	0.0190	0.0574	0.1516
d_{MAE} [Nm]	0.7856	2.3440	–
$\theta_{s\text{RMSE}}$ [rad]	0.0007	0.0060	0.0120
$\omega_{w\text{RMSE}}$ [rpm]	0.0241	0.0830	0.2929
d_{RMSE} [Nm]	1.8189	4.1963	–

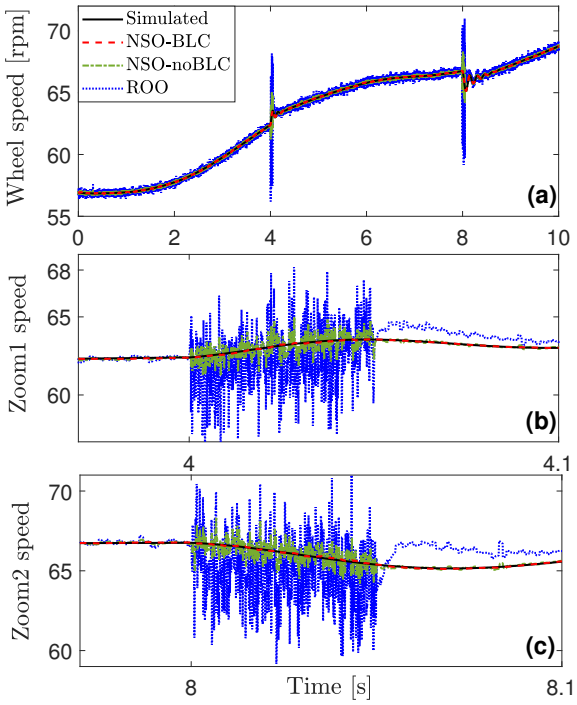

Fig. 12: Scenario 2. (a) estimation of the wheel speed ω_w, (b) zoom at the first gear-shifting, (c) zoom at the second gear-shifting.

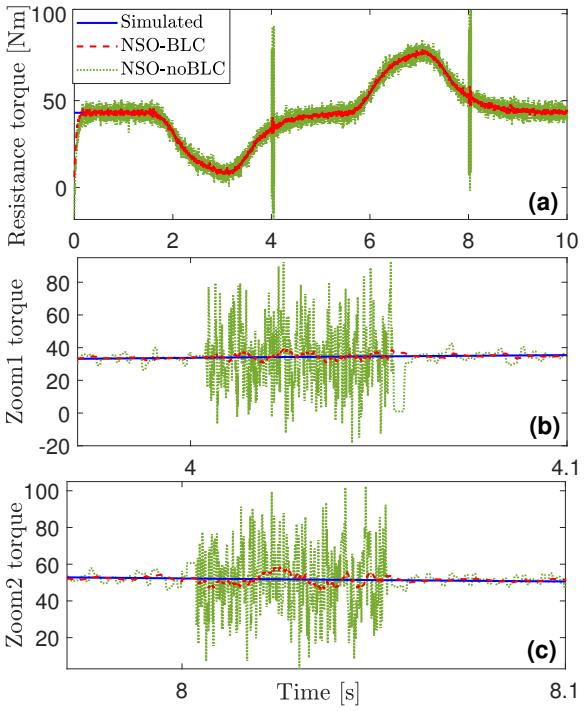

Fig. 13: Scenario 2. (a) estimation of the resistance load torque T_d, (b) zoom at the first gear-shifting, (c) zoom at the second gear-shifting.

V. Conclusions

A new method has been proposed to simultaneously estimate the unmeasured torsion angle and wheel rotation speed as well as the unknown resistance torque of IMT systems, which can be reformulated as nonlinear switched models. To this end, we propose a nonlinear switched observer structure, being able to reconstruct both state and unknown input. The

nonlinear mismatching term involved in the estimation error dynamics is handled by the mean value theorem. Employing Lyapunov stability theorem, sufficient LMI conditions are derived to design nonlinear observers while guaranteeing an ℓ_∞ performance. Moreover, we propose a bumps limitation constraint, expressed in terms of LMIs, that can be directly incorporated to the observer design conditions. Hence, the negative impact of switching discontinuities is significantly reduced compared to related estimation methods, especially under the effect of sensor noises. Illustrative estimation results and comparative studies are performed with realistic test scenarios to show the interests of the new method. Future works extend the proposed switched observer structure for nonlinear fault-tolerant control of IMT systems in presence of motor faults and unknown inputs. Real-time validations are also necessary to confirm the practical estimation performance of the proposed estimation method.

REFERENCES

[1] G. Du, W. Cao, S. Hu, Z. Lin, and T. Yuan, "Design and assessment of an electric vehicle powertrain model based on real-world driving and charging cycles," *IEEE Trans. Veh. Technol.*, vol. 68, no. 2, pp. 1178–1187, 2019.

[2] G. Ma, M. Ghasemi, and X. Song, "Integrated powertrain energy management and vehicle coordination for multiple connected hybrid electric vehicles," *IEEE Trans. Veh. Technol.*, vol. 67, no. 4, pp. 2893–2899, 2018.

[3] M. Zulkefli and Z. Sun, "Fast numerical powertrain optimization strategy for connected hybrid electric vehicles," *IEEE Trans. Veh. Technol.*, vol. 68, no. 9, pp. 8629–8641, 2019.

[4] Y. Liu, D. Gao, K. Zhai, Q. Huang, Z. Chen, and Y. Zhang, "Coordinated control strategy for braking and shifting for electric vehicle with two-speed automatic transmission," *eTransportation*, vol. 13, p. 1018, 2022.

[5] Z. Zhou and R. Guo, "A disturbance-observer-based feedforward-feedback control strategy for driveline launch oscillation of hybrid electric vehicles considering nonlinear backlash," *IEEE Trans. Veh. Technol.*, vol. 71, no. 4, pp. 3727–3736, 2022.

[6] M. Hu, J. Zeng, S. Xu, C. Fu, and D. Qin, "Efficiency study of a dual-motor coupling EV powertrain," *IEEE Trans. Veh. Technol.*, vol. 64, no. 6, pp. 2252–2260, 2015.

[7] X. Zhu, Z. Hui, D. Cao, and Z. Fang, "Robust control of IMT powertrain system over controller area network for automotive applications," *Mech. Syst. Signal Process.*, vol. 58, pp. 15–28, 2015.

[8] X. Zhu and W. Li, "Takagi–Sugeno fuzzy model based shaft torque estimation for integrated motor–transmission system," *ISA Trans.*, vol. 93, pp. 14–22, 2019.

[9] Y. Tian, J. Ruan, N. Zhang, J. Wu, and P. Walker, "Modelling and control of a novel two-speed transmission for electric vehicles," *Mech. Mach. Theory*, vol. 127, pp. 13–32, 2018.

[10] L. Glielmo, L. Iannelli, V. Vacca, and F. Vasca, "Gearshift control for automated manual transmissions," *IEEE/ASME Trans. Mechatron.*, vol. 11, no. 1, pp. 17–26, 2006.

[11] K. Sugiura and Y. Hori, "Vibration suppression in 2- and 3-mass system based on the feedback of imperfect derivative of the estimated torsional torque," *IEEE Trans. Indus. Electron.*, vol. 43, no. 1, pp. 56–64, 1996.

[12] R. Mousavi, V. Alizadeh, and B. Boulet, "Estimation of synchromesh frictional torque and output torque in a clutchless automated manual transmission of a parallel hybrid electric vehicle," *IEEE Trans. Veh. Technol.*, vol. 66, no. 7, pp. 5531–5539, 2017.

[13] M. Li, Z. Zhao, J. Fan, and J. Gao, "Estimation of transmission input-output shaft torque and drive wheel speed for compound power split powertrain based on unknown input observer," *IEEE Trans. Veh. Technol.*, vol. 69, no. 5, pp. 4883–4893, 2020.

[14] H. Flieh, E. Totoki, and R. Lorenz, "Dynamic shaft torque observer structure enabling accurate dynamometer transient loss measurements," *IEEE Trans. Indus. Appl.*, vol. 54, no. 6, pp. 6121–6132, 2018.

[15] J. Na, S. Chen, G. Herrmann, R. Burke, and C. Brace, "Vehicle engine torque estimation via unknown input observer and adaptive parameter estimation," *IEEE Trans. Veh. Technol.*, vol. 67, no. 1, pp. 09–22, 2018.

[16] J. Kim and S. Choi, "Nonlinear torque observer for a self-energizing clutch actuator using a reaction torque estimation approach," *IEEE/ASME Trans. Mechatron.*, vol. 20, no. 6, pp. 3071–3084, 2015.

[17] D. Xu, J. Zhang, B. Zhou, and H. Yu, "Robust hierarchical estimator of clutch torques for a compound power-split hybrid electric vehicle," *Mech. Syst. Signal Process.*, vol. 134, p. 106320, 2019.

[18] J. Baumann, D. Torkzadeh, A. Ramstein, U. Kiencke, and T. Schlegl, "Model-based predictive anti-jerk control," *Control Eng. Pract.*, vol. 14, no. 3, pp. 259–266, 2006.

[19] L. Marcos and M. Terra, "Markovian filtering for driveshaft torsion estimation in heavy vehicles," *Control Eng. Pract.*, vol. 12, p. 145, 2020.

[20] T. Pan, H. Zang, P. Qiang, and P. Wu, "Dual-objective torque control of electric vehicles drivetrain with robust global finite-time stability guarantee," *Veh. Syst. Dyn.*, pp. 1–24, 2022.

[21] J. Pan, A.-T. Nguyen, T.-M. Guerra, and D. Ichalal, "A unified framework for asymptotic observer design of fuzzy systems with unmeasurable premise variables," *IEEE Trans. Fuzzy Syst.*, vol. 29, no. 10, pp. 2938–2948, 2021.

[22] T. Lee, D.-H. Kim, and S. Choi, "Driveline modeling with transmission loss and robust torque observer design for dual clutch transmission," *IEEE Trans. Veh. Technol.*, vol. 71, no. 2, pp. 1267–1279, 2022.

[23] P. Li, A.-T. Nguyen, H. Du, Y. Wang, and H. Zhang, "Polytopic LPV approaches for intelligent automotive systems: State of the art and future challenges," *Mech. Syst. Signal Process.*, vol. 161, p. 107931, 2021.

[24] H. Chen, S. Lou, and C. Lv, "Hybrid physics-data-driven online modelling: Framework, methodology and application to electric vehicles," *Mech. Syst. Signal Process.*, vol. 185, p. 109791, 2023.

[25] S. Boyd, L. El Ghaoui, E. Feron, and V. Balakrishnan, *Linear Matrix Inequalities in System and Control Theory*. Philadelphia, PA: SIAM, 1994, vol. 15.

[26] J.-W. Zhu, G.-H. Yang, H. Wang, and F. Wang, "Fault estimation for a class of nonlinear systems based on intermediate estimator," *IEEE Trans. Autom. Control*, vol. 61, no. 9, pp. 2518–2524, 2016.

[27] B. Zhang, H. Du, J. Lam, N. Zhang, and W. Li, "A novel observer design for simultaneous estimation of vehicle steering angle and sideslip angle," *IEEE Trans. Indus. Electron.*, vol. 63, no. 7, pp. 4357–4366, 2016.

[28] A.-T. Nguyen, T. Dinh, T.-M. Guerra, and J. Pan, "Takagi–Sugeno fuzzy unknown input observers to estimate nonlinear dynamics of autonomous ground vehicles: Theory and real-time verification," *IEEE/ASME Trans. Mechatron.*, vol. 26, no. 3, pp. 1328–1338, 2021.

[29] J. Pan, A.-T. Nguyen, T.-M. Guerra, C. Sentouh, S. Wang, and J.-C. Popieul, "Vehicle actuator fault detection with finite-frequency specifications via Takagi-Sugeno fuzzy observers: Theory and experiments," *IEEE Trans. Veh. Technol.*, pp. 1–11, 2022.

[30] Y. Li, M. Yuan, M. Chadli, Z.-P. Wang, and D. Zhao, "Unknown input functional observer design for discrete-time interval type-2 Takagi–Sugeno fuzzy systems," *IEEE Trans. Fuzzy Syst.*, vol. 30, no. 11, pp. 4690–4701, 2022.

[31] Q. Jia, W. Chen, Y. Zhang, and H. Li, "Fault reconstruction and fault-tolerant control via learning observers in Takagi–Sugeno fuzzy descriptor systems with time delays," *IEEE Trans. Indus. Electron.*, vol. 62, no. 6, pp. 3885–3895, 2015.

[32] B. Gao, Q. Liang, Y. Xiang, L. Guo, and H. Chen, "Gear ratio optimization and shift control of 2-speed I-AMT in electric vehicle," *Mech. Syst. Signal Process.*, vol. 50, pp. 615–631, 2015.

[33] S. Ding, *Model-Based Fault Diagnosis Techniques: Design Schemes, Algorithms, and Tools*. Springer Science & Business Media, 2008.

[34] B. Jiang, M. Staroswiecki, and V. Cocquempot, "Fault accommodation for nonlinear dynamic systems," *IEEE Trans. Autom. Control*, vol. 51, no. 9, pp. 1578–1583, 2006.

[35] D. Zhao, Z. Wang, Q.-L. Han, and G. Wei, "Proportional–integral observer design for uncertain time-delay systems subject to deception attacks: An outlier-resistant approach," *IEEE Trans. Syst. Man Cybern. Syst.*, vol. 52, no. 8, pp. 5152–5164, 2022.

[36] Y. Mu, H. Zhang, R. Xi, Z. Wang, and J. Sun, "Fault-tolerant control of nonlinear systems with actuator and sensor faults based on T–S fuzzy model and fuzzy observer," *IEEE Trans. Syst., Man, Cybern., Syst.*, vol. 52, no. 9, pp. 5795–5804, 2022.

[37] D. Liberzon, *Switching in Systems and Control*. Boston: Birkhauser: Springer, 2003, vol. 190.

[38] J. Daafouz, J. Geromel, and G. Deaecto, "A simple approach for switched control design with control bumps limitation," *Syst. Control Lett.*, vol. 61, no. 12, pp. 1215–1220, 2012.

[39] J. Löfberg, "YALMIP: A toolbox for modeling and optimization in Matlab," in *Proc. IEEE Int. Symp. CACSD*, Taipei, 2004, pp. 284–289.